Residual Stress Effects on Fatigue and Fracture Testing
J.O. Bunch, M.R. Mitchell, Editors
ASTM, Lancaster, PA STP1497
Pgs. 69-84, January 2007

FULL PAPER

P. Prevéy,[1] *N. Jayaraman,*[2]

A Design Methodology to Take Credit for Residual Stresses in Fatigue Limited Designs

ABSTRACT: High cycle fatigue (HCF) performance of turbine engine components has been known for decades to benefit from compressive surface residual stresses produced by shot peening. Recently laser shocking and low plasticity burnishing (LPB) have been shown to provide spectacular fatigue and damage tolerance improvement by introducing deep or through-thickness compression in fatigue critical areas. However, the lack of a comprehensive design method that defines the depth and magnitude of compression required to achieve a design fatigue life has prevented surface enhancement from being used for more than a safeguard against HCF damage initiation. The present paper describes a design methodology and testing protocol to allow credit to be taken for the beneficial compression introduced by surface enhancement in component design to achieve a required or optimal fatigue performance.

A detailed design method has been developed that relates the required fatigue life, the mean and alternating applied stresses, and the damage in terms of K_f to the residual stress at the fatigue initiation site required for the targeted HCF performance. The method is applied to feature specimens designed to simulate the fatigue conditions in the trailing edge of a 1st stage low pressure Ti-6-4 compressor vane to provide the optimal trailing edge damage tolerance. A novel adaptation of the traditional Haigh diagram to estimate the compressive residual stress magnitude for optimal fatigue performance is introduced. Fatigue results on blade-edge feature samples are compared with analytical predictions provided by the design methodology.

KEYWORDS: residual stress, design, Haigh diagram, fatigue, high cycle fatigue (HCF)

INTRODUCTION

Residual compressive stresses in metallic components have long been recognized[1-4] to enhance fatigue strength. Engineering components have been shot-peened or cold worked to create a surface layer of residual compressive stress with fatigue strength enhancement as the primary objective, or as a by-product of a surface hardening treatment like carburizing, nitriding, induction hardening, etc. Over the last decade, additional surface enhancement methods including LPB,[5] laser shock peening (LSP),[6] and ultrasonic peening have emerged. These surface treatment methods have been shown to improve the fatigue performance of engineering components to different degrees.

LPB has been demonstrated to provide a deep (~1mm), thermally and mechanically stable, surface layer of high magnitude compression in various aluminum, titanium, and nickel based alloys, and steels. Thermal and mechanical stability are obtained when compression is introduced with minimal cold working of the surface. A deep stable compressive residual stress state on the surface of these materials has been shown to be effective in mitigating fatigue

[1] President, Director of Research, Lambda Research, 5521 Fair Lane, Cincinnati, OH 45227
[2] Director of Materials Research, Lambda Research, 5521 Fair Lane, Cincinnati, OH 45227

damage due to foreign object damage (FOD),[7,8] fretting,[9] corrosion fatigue[10], and corrosion pitting.[11]

Because the shallow layer of compression produced by shot peening is easily damaged and may not be retained in service, designers have used shot peening primarily for added safety, and have not taken credit for the fatigue benefits in design methodology. In contrast, LPB and LSP produce thermally and mechanically stable compression over 1 mm deep, providing reliable mitigation of the fatigue debit of FOD, fretting, and corrosion pits. In high strength alloys, the original fatigue performance of the virgin material is achieved even in the presence of typical service generated defects. In the absence of compressive residual stresses, the allowable damage is generally limited to a fatigue notch sensitivity factor, k_f, on the order of 3. This design constraint leads to low allowable design stresses and hence much heavier sections.

Although mitigation of FOD, pitting, fretting and corrosion damage has been demonstrated, a comprehensive approach to designing structures by taking specific design credit for surface compressive residual stresses has not been developed. Additional design factors including the compensatory tension necessary for equilibrium and distortion due to the introduction of residual compression into the structure must also be taken into account in this design process. This paper proposes a design approach suitable for structural alloys in high cycle fatigue and provides a specific case study of HCF behavior of Ti-6Al-4V feature specimens designed to simulate the stress conditions in an aircraft engine 1st stage compressor vane.

STRESS-LIFE ANALYSIS:

The Haigh diagram[12], or constant fatigue life diagram, widely used to illustrate the effects of mean stresses on fatigue life, is shown in Figure 1 as a map of the allowable stresses for a constant cyclic life in high cycle fatigue plotted as solid lines for a given alloy system. It is customary to plot the allowable alternating stress as the ordinate for a given mean stress on the abscissa, with the stress ratios $R = \sigma_{min}/\sigma_{max}$ shown as radial lines. The stress axes may be normalized with respect to the tensile strength of the material. The Haigh diagram, a convenient graphical representation to show the effects of mean stress, is usually prepared from experimental fatigue test results.

Effects of the notch fatigue sensitivity factor (k_f = unnotched σ_e / notched σ_e), where σ_e is the endurance limit or fatigue strength for a given life at R=-1, are also plotted as dotted lines in Figure 1, again based upon experimental results. Although Haigh's fatigue tests included compressive mean stresses, the Haigh diagrams shown subsequently in the fatigue literature usually did not include the compressive mean stress range.

Fatigue life predictive models, including the Goodman, Gerber and Soderberg constant life curves, can be plotted on the Haigh diagram as functions of alternating stress amplitude plotted against mean stress, as shown schematically in Figure 2. Correspondingly,

$$\sigma_a = \sigma_e \{1 - \sigma_m/\sigma_{YS}\} \quad \text{Soderberg} \quad [1]$$

$$\sigma_a = \sigma_e \{1 - \sigma_m/\sigma_{UTS}\} \quad \text{Goodman} \quad [2]$$

$$\sigma_a = \sigma_e \{1 - (\sigma_m/\sigma_{UTS})^2\} \quad \text{Gerber} \quad [3]$$

where σ_a is the allowable alternating stress, σ_e is the fatigue strength at R ($\sigma_{min}/\sigma_{max}$) = -1 and σ_m is the mean stress at which the allowable alternating stress is to be determined. Thus, these predictive models give the allowable alternating stress for a predetermined cyclic life (say, 10^7 cycles) knowing only the fatigue strength in fully-reversed cyclic loading, the mean stress, and the yield or tensile strength of the material.

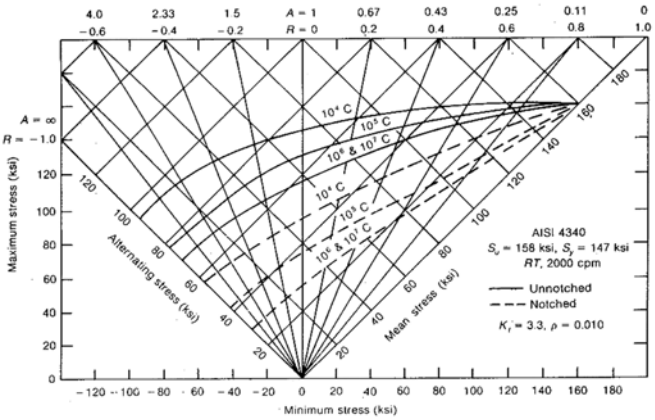

FIG. 1 – Haigh diagram for establishing influence of mean stress in fatigue for AISI 4340 steel for fatigue lives from 10^4 to 10^7 cycles, k_f = 1 and k_f=3.3. (from MIL-HBDK-5, US Dept. of Defense, Dieter (1986), Mechanical Metallurgy, McGraw-Hill, Third Edition pg. 386, Figure 12-9.)

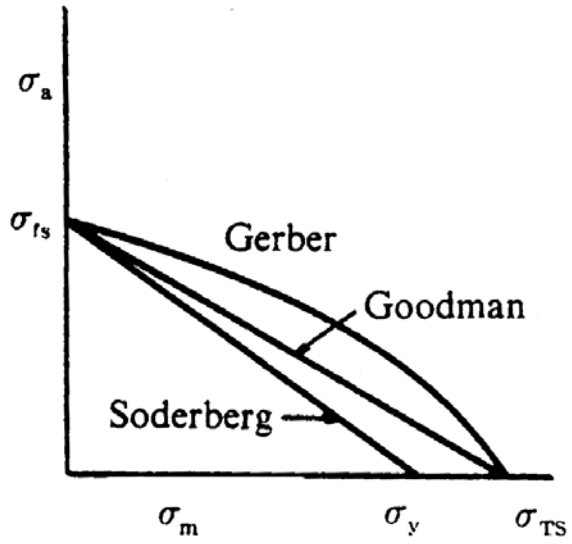

FIG. 2 – Constant life curves for fatigue loading with nonzero mean stress. (Suresh (1998), Fatigue of Materials, Cambridge University Press, Second Edition, pg. 226, Figure 7.4 (b))

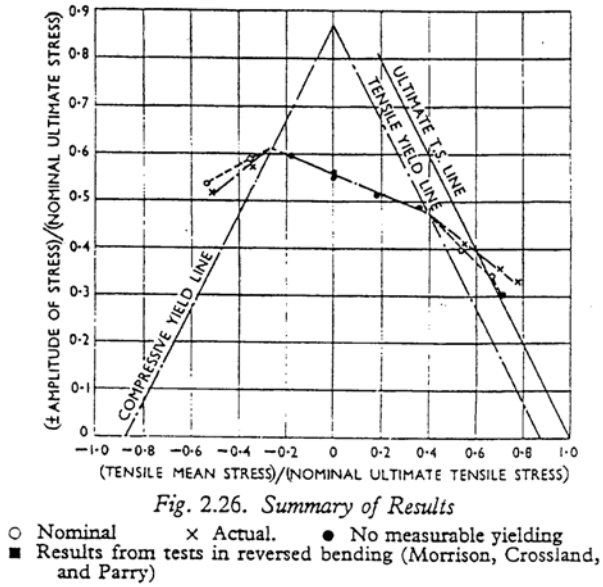

Fig. 2.26. Summary of Results

○ Nominal × Actual. ● No measurable yielding
■ Results from tests in reversed bending (Morrison, Crossland, and Parry)

FIG. 3 – Haigh diagram for alloy steel showing yield strength limits in both tension and compression. (H.C. O'Connor, J.L.M. Morrison, (1956), "The Effect of Mean Stress on the Push-Pull Fatigue Properties of an Alloy Steel," Intn'l Conf. on Fatigue, Inst. Of Mechanical Engineers, pg. 108, Figure 2.26.)

Early HCF experimental work attempted in the 1950s and 1960s with compressive mean stresses at R < -1 met with limited success primarily due to difficulties with specimen alignment when testing in compression.[13-16] Although test methods have improved, and perhaps due to the a primary interest in tensile mean stresses in design, the literature contains little HCF data for high negative R suitable to extend the Haigh diagram into the compressive mean stress region. O'Conner and Morrison[13] constructed a Haigh diagram for an alloy steel, shown in Figure 3, with a triangular bounding region to indicate the limits of applied alternating stress, for both tensile and compressive mean stress, up to the yield strength stress limits.

Because of the limited availability of data for R < -1, Haigh diagrams are seldom used to predict the fatigue performance under compressive mean stresses. Engineering design approaches that include compressive mean stresses as part of the global structurally applied stresses are rare. Therefore, other than for academic curiosity, there has not been a serious need for fatigue predictions under compressive mean loads. The lack of reliable fatigue life prediction methods has further limited the ability to take credit for compressive residual stresses in design.

With the recognition of the fatigue improvement achievable with surface enhancement treatments, there is a need for predicting fatigue behavior with compressive mean stresses. In the following section, the application of a simple stress-strain function to unify available HCF data for different R-ratios and k_f values is developed. The resulting fatigue design diagram is a modified Haigh diagram extended to include compressive mean stresses. The proposed fatigue design diagram enables: (a) prediction of fatigue behavior in the presence of damage, (b) prediction of fatigue behavior in the presence of both damage and residual stresses, and (c) more importantly, provides a design guideline to determine the compressive residual stress magnitude needed to achieve a target damage tolerance. The fatigue design diagram provides a design tool to allow credit to be taken for residual compressive stress distributions in the design of fatigue critical components.

Model Development:

Smith, Watson and Topper[17] (SWT) suggested a single stress-strain function,

$$\sqrt{(\sigma_{max}\varepsilon_{alt}E)} = \text{constant} \qquad [4]$$

to combine the effects of mean stress and alternating stress. They demonstrated that this function, when plotted against log(N_f), effectively unified the fatigue results for tensile and compressive mean stresses in SAE1015 steel, 2024-T4 Al alloy, SAE4340 steel and 24S-T3 Al alloy. Assuming that elasticity conditions dominate high cycle fatigue (and therefore, $\varepsilon_{alt}E = \sigma_{alt}$,) Fuchs and Stephens[18] considered application of the stress function,

$$\sqrt{(\sigma_{max}\sigma_{alt})} = \text{constant} \quad [5]$$

in place of the stress-strain function in HCF. Additionally, the effect of notches can be included by considering the Neuber's rule expressed in terms of $k_f \leq k_t$ for the practical range of design where $1 < k_t < 4$,

$$\sigma\varepsilon = k_f^2 S_e \quad [6]$$

where σ and ε represent the notch root stress and strain, S and e represent the nominal stress and strain, and k_t is the tensile notch sensitivity factor. The combination of the stress function, $\sqrt{(\sigma_{max}\sigma_{alt})}$ and Neuber's rule in the essentially elastic HCF stress range leads to a new stress function

$$k_f\sqrt{(S_{max}S_{alt})} = \text{constant} \quad [7]$$

Since $S_{max} = S_{mean} + S_{alt}$, the unifying stress function including the notch effects can be written as

$$k_f^2(S_{mean} + S_{alt})S_{alt} = \text{constant} \quad [8]$$

In the limiting case of $k_f = 1$ and $S_{mean} = 0$, the stress function is simply S_e^2, where S_e is the nominal fatigue strength under fully-reversed cyclic loading (R = -1) conditions. Therefore,

$$k_f^2(S_{mean} + S_{alt})S_{alt} = S_e^2 \quad [9]$$

Based on the above analysis, it is possible to theoretically construct a series of Haigh diagrams for various k_f values, simply based upon a single fatigue strength value, S_e for the material. Further, the series of lines when plotted within the bounds of the yield strength triangle, provides the engineering design limits. Fuchs and Stephens, when plotting this triangle, chose to use the cyclic yield stress for the maximum allowable alternating stress at the apex of the triangle. Because the allowable stress limits are much less than the either yield strength in HCF limited designs, for the purposes of the present discussion, the difference between the yield limits is not significant, and the exact location of the yield boundaries are of interest only at extreme design limits.

The fatigue design diagram for Ti-6Al-4V is presented in Figure 4 as a plot of S_{alt} vs S_{mean}, with the yield strength triangle indicating the elastic limits. Fatigue strength data from Aerospace Structural Metals Handbook[19] for k_t ($\approx k_f$) values of 1 and 2.82 are plotted for R of –1, 0 and 0.5 in Figure 5. The results from 4-point bending fatigue tests conducted at Lambda Research are also plotted. For the sake of reference, constant R lines for R=0.1, R=-1 and R=-2 are also plotted.

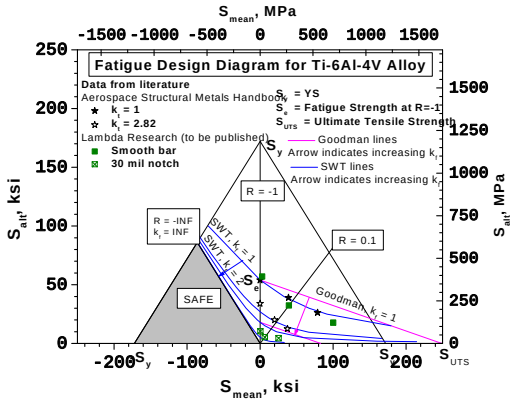

FIG. 4 – Fatigue design diagram for Ti-6Al-4V showing allowed alternating and mean stresses for 10^7 cycle life for different R-ratios and fatigue notch sensitivity factors k_f.

Goodman lines for k_f=1 and k_f=3 were constructed using the endurance limit at R=-1 and true fracture strength value from the Aerospace Structural Metals Handbook. Similarly, the modified SWT lines are plotted using the above equation and the single fatigue strength value, S_e at R of –1 for the smooth bar. The modified SWT line for k_f=2 shows a substantial debit in fatigue performance. The lines for k_f=3 and beyond practically converge in both the compressive and tensile mean stress regimes. For $k_f \geq 5$, and for the limiting notch condition (k_f approaching ∞), the modified SWT line coincides with R=-∞ in the compressive mean stress region, and shows practically no allowable alternating stress in the tensile mean stress regime. In the region to the left of the R=-∞ line, the part is entirely in compression throughout the loading cycle. If the assumption that fatigue damage and failure by crack propagation (mode I crack propagation) is not possible in the absence of a cyclic tensile stress component, then there exists a safe triangular region where no fatigue damage is possible. This triangular

region is marked "SAFE" in the fatigue design diagram.

For the sake of completeness, additional data from ML and ASE[20] from the HCF annual Report Section 2.2 are shown in Figure 5. As seen in this figure, there is general agreement between different sources of fatigue data in the mean stress regime corresponding to R≥ 0, while in the mean stress regime with R<0, there is some significant scatter in the data, and the modified SWT line is conservative, in that it under-predicts the fatigue strength.

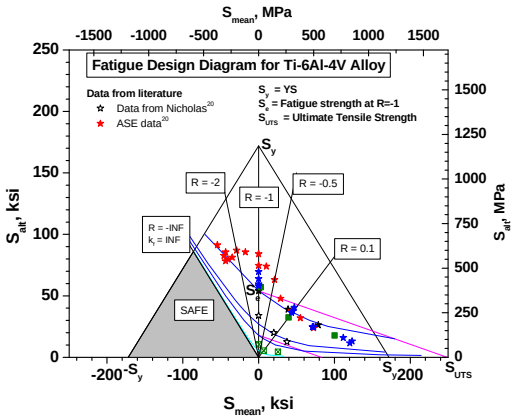

FIG. 5 - Same as Figure 4, with the inclusion of additional experimental data (smooth bar results) from reference 20, showing reasonable agreement for R<-2 and R> -0.5

Prediction Method:

In using this fatigue design diagram to estimate the allowable mean and alternating stresses, only the stresses in the region where fatigue damage initiates are of interest. For example, if fatigue damage initiation occurs at a corrosion pit, FOD, or other surface damage, the local stresses in the affected region are of interest, including the immediate sub-surface region. The knowledge of the applied stresses, R, and the depth of damage to be tolerated (and resulting k_f) are needed to determine the appropriate surface residual stress magnitude for a successful design. In the absence of a specified target depth of damage tolerance, the maximum possible damage tolerance may be assumed.

In this section, a hypothetical case is discussed with the help of a magnified section of the fatigue design diagram from Figure 6a. Let us assume that the part is subjected to fatigue loading at an R=0.1. The modified SWT line for k_f=1 (no surface defects) predicts a nominal mean stress of 300 MPa (44 ksi) and a nominal alternating stress of 250 MPa (36 ksi) plotted as point A in Figure 6a. In the presence of defects such that k_f=3, these stresses drop to nominally 106 and 87 MPa (15.4 and 12.6 ksi), respectively moving the allowed operating point to point B along the R=0.1 line. In order to achieve full mitigation of the damage and restore the fatigue strength in the presence of the k_f=3 conditions, the surface mean stress (residual plus applied) must be moved into higher compression along the k_f=3 modified SWT line up to the point C. The difference in the mean stress of point C with respect to point B (i.e., the distance BD in Figure 6a) represents the amount of surface compressive residual stress needed to fully mitigate the surface damage. This compressive residual stress magnitude is needed at the point of fatigue crack initiation at the bottom edge of the damage.

In a second example, consider a fatigue loading condition of R=-1. Under this condition, (Point A in Figure 6b) the modified SWT line for k_f=1 (smooth surface) predicts a S_{alt} of 370 MPa (54 ksi) with a zero mean stress. For the limiting FOD condition as k_f approaches infinity, corresponding to even a modest size crack or notch, the fatigue strength becomes negligible (Point B in Figure 6b). In order to fully mitigate even this extreme condition, residual compression can be introduced into the surface at the depth of the FOD or crack tip sufficient to move along the k_f=∞ modified SWT line to point C. Again, the difference in the mean stress of Point C with respect to Point B (i.e., the distance BD in Figure 6b) represents the amount of surface compressive residual stress, nominally –400 MPa (-58 ksi), needed to fully restore the fatigue strength with the damage present. Again, this compressive residual stress must exist in the region covering the tip of the defect or crack from which fatigue cracks will originate.

Case Study of Mitigating FOD in blade-edge simulation feature specimens:

The following examples are taken from a study involving a HCF of blade-edge feature specimens designed to simulate the fatigue conditions experienced by the edge of a compressor vane in a turbine engine. Figures 7(a) and (b) show two specimen designs for HCF testing at R=0.1 and –1, respectively, chosen to investigate the effect of stress ratio on HCF behavior. All HCF tests were run at room temperature in 4-point bending on a Sonntag SF-1U fatigue machine at 30 Hz with the specimens loaded in the hard-bending mode (edges, not sides, under maximum stress). FOD was simulated with electrical discharge machining (EDM) notches ranging from 0.25 to 2.5 mm (0.010 to 0.100 in.) deep machined into the edges of the specimens as shown in figures 7 (a) and (b).

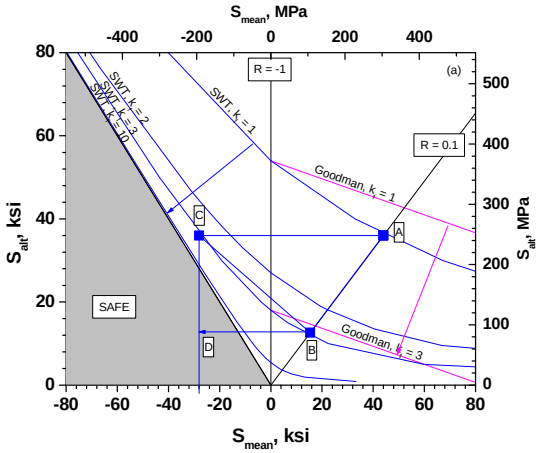

(a)

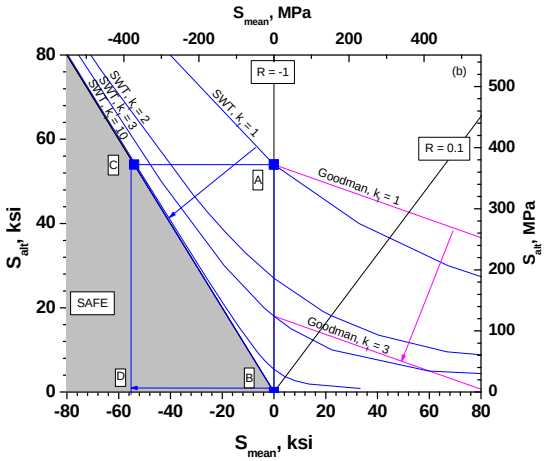

(b)

FIG. 6 - Magnified sections of the fatigue design diagram illustrating the fatigue design process with residual stresses in the presence of defects (FOD, pits or cracks). (a) Illustrates the effect of compressive stress (BD) to mitigate $k_f = 3$ for a fatigue condition of R=0.1 and in (b) the effect of compressive stress (BD) to mitigate a $k_f = \infty$ is shown.

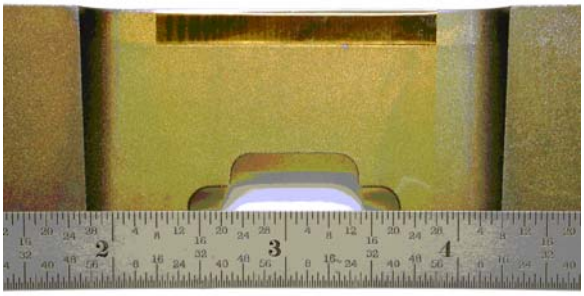

FIG. 7(a)

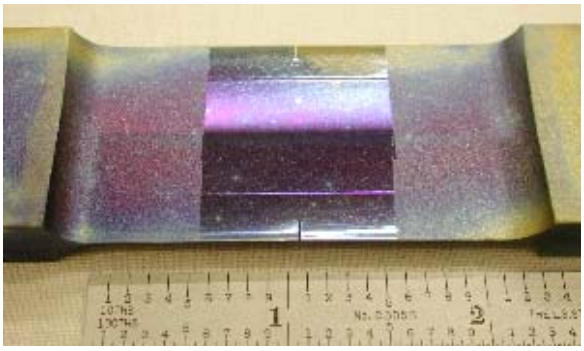

FIG. 7(b)

FIG. 7 - (a) Single Edge Blade (SEB) and (b) Double Edge Blade (DEB) feature specimens used for simulation of HCF damage in the trailing edge at R=0.1 and –1, respectively.

The specimen edges were LPB treated to impart through-thickness compressive residual stresses. Residual stresses were measured by x-ray diffraction methods, and the residual stress distributions are plotted in Figure 8. This figure shows the full residual stress map as a function of distance (chord-wise) from the edge of the specimen at the various depths indicated. Subsurface measurements were obtained by electrochemical polishing to remove layers up to the mid-thickness of the specimen before x-ray measurements, and the results were corrected for stress relaxation. The minimum compression occurs at mid-thickness, and fatigue failure initiated from this region. In Figure 8, the residual stress results are shown spanning the LPB treated region and into the region of compensatory tension developed behind the LPB processed regions. The maximum compensatory tension of 220 MPa (~ 32 ksi) occurs in the mid plane of the specimen just behind the LPB processed region. Compensatory tensile stresses near the surface are lower. A discussion of the incorporation of compensatory tension into design is presented later in this paper.

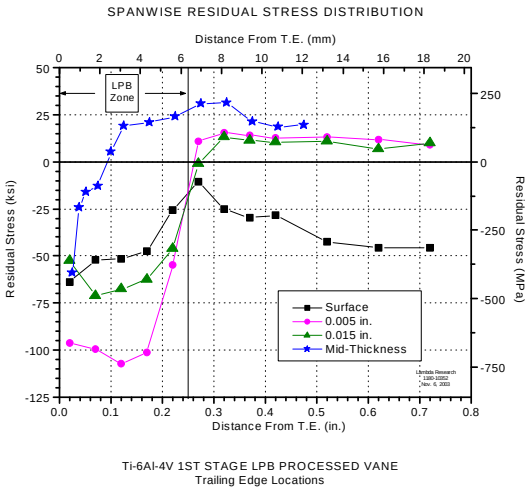

FIG. 8 - Residual stress map of the LPB processed vane obtained by x-ray diffraction measurements of the spanwise residual stress at various distances from the trailing edge and depths from the surface.

The HCF test results are shown in Figure 9 as S-N plots for both single-edge samples tested at R=0.1 and double-edge samples tested at R=-1. Although HCF tests were performed for a variety of FOD depths, for the sake of brevity and clarity, only the results from FOD of 0.5 mm (0.020 in.) depth are presented. In the presence of 0.5 mm deep FOD, the baseline (untreated) fatigue strengths at R = 0.1 and –1 are nominally 70 and 105 MPa (10 and 15 ksi), respectively. As indicated in Figure 9, none of the LPB treated specimens with 0.5 mm FOD tested at either stress ratio failed from the FOD. The fatigue performance of the LPB treated specimens was substantially better than the baseline specimens for either stress ratio and sample design, indicating that the LPB treatment largely mitigated the adverse effects of the 0.5 mm deep FOD. However, most of the specimens failed by sub-surface crack initiation from the mid-plane, or in regions of the specimen away from the FOD as shown in Figures 10a and b. The variation in the depth and location of the fatigue initiation introduced scatter into the results, in spite of the presence of simulated FOD. Estimates of the 10^7 cycle fatigue strength corresponding to the two dominant failure modes (initiation from FOD vs sub-surface initiation), are shown as upper-bound and lower-bound S-N curves for the experimental data in Figure 9. The fatigue strength for LPB treated specimens with a 0.5 mm (0.020 in.) FOD at R = 0.1 was estimated to be nominally 725 MPa (105 ksi), and at R = -1, nominally 380 MPa (55 ksi). The corresponding fatigue strengths for subsurface failure initiation are estimated to be nominally 480 and 310 MPa (70 and 45 ksi,) respectively.

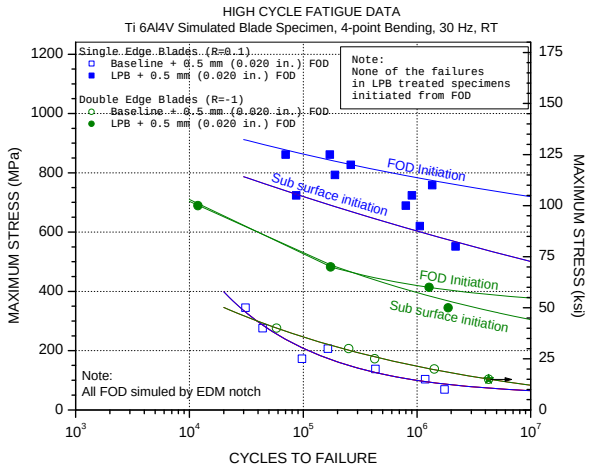

FIG. 9 - HCF test results for the blade edge simulation feature specimens.

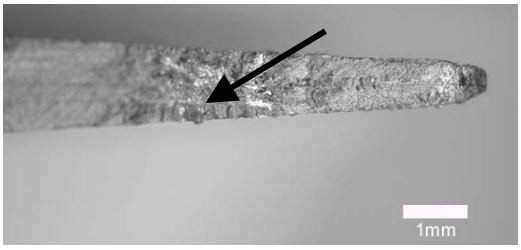

(a)

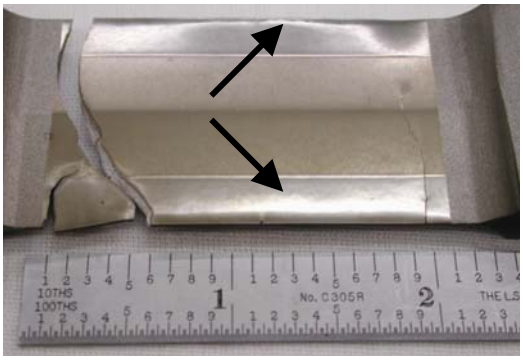

(b)

FIG. 10 - (a) Optical fractograph of a SEB feature specimen with LPB treatment showing crack initiation from sub surface regions (arrow). LPB + 0.5 mm (0.020 in) FOD, R=0.1 σ_{max}=690 MPa (100 ksi), N_f = 800,038 cycles, (b) Failure of a DEB feature specimen with LPB treatment showing initiation in a remote area in spite of the presence of 0.5 mm (0.020 in.) FOD (arrows) on both edges of the specimen. R=-1, σ_{max} = 480 MPa (70 ksi,) N_f = 174,315 cycles.

The baseline fatigue strengths, plotted on the fatigue design diagrams as Points B in Figures 11a and 12a, correspond to nominal fatigue notch sensitivity factors, k_f, of 10 and 3.4, respectively. This difference in k_f for the same notch size may be attributed to the fatigue cycling conditions (tension-tension for R = 0.1, and tension-compression for R = -1). Now, given the least compressive residual stress of -413 MPa (-60 ksi) produced by LPB at mid-thickness and the 0.5 mm (0.020 in.) FOD depth, the points B can be translated to points C along the respective modified SWT lines. Positions C in Figures 11a and 12a represent the actual stress state at the tip of the FOD. The allowed applied stresses are then given by the points E, that represent the predicted fatigue performance of these specimens with the additional compressive residual stress indicated by the shift from B to D along the means stress axis. The measured fatigue strengths (from Figure 9) of 725 MPa (105 ksi) for R = 0.1, and 380 MPa (55 ksi) for R = -1, in the absence of compensatory tension, are plotted in Figures 11a and 12a as points F (Actual).

However, none of the LPB treated specimens actually failed from the EDM simulated FOD. The failures originated from sub-surface crack initiation at the depth where the compensatory tensile stresses were maximum. The fatigue strengths associated with this damage mechanism for R = 0.1 and R = -1 are estimated to be 480 MPa (70 ksi) and 310 MPa (45 ksi), respectively. When the maximum sub-surface compensatory tension at 220 MPa (32 ksi) at mid-thickness of the specimen is introduced into the fatigue design diagram analysis, the fatigue performance predictions are presented in Figures 11b and 12b. Here, since there are no preexisting flaws from which the cracks initiate, the effective k_f is considered to be 1, and therefore the modified SWT line corresponding to a k_f=1 was used for this analysis. Starting from the baseline positions of "B" in both Figures 11b and 12b, and accounting for the mid-thickness compensatory tension of 220 MPa (32 ksi), corresponding to distance BD in Figures 11b and 12b, the stress state is translated to positions C. Since the entire specimen is subjected to fatigue cycling at R of 0.1 and –1, the predicted fatigue strengths with the subsurface compensatory tension are marked by points E in Figures 11b and 12b. Again, in both Figures 11b and 12b, the corresponding measured fatigue strengths of 480 MPa (70 ksi) and 310 MPa (45 ksi) are also indicated by points F (Actual). It is evident from these figures that the predicted fatigue strengths are lower than the predictions from 11a and 12a. Therefore, the preferred failure mechanism is sub-surface crack initiation, as observed in testing. It is also evident that in the absence of the compressive residual stresses, the fatigue strengths would have been 10 ksi and 15 ksi, respectively, plotted as points X in Figures 11b and 12b. Even with sub-surface crack initiation from the region of maximum compensatory tension, the fatigue strengths of the specimens with LPB treatments were increased by a factor of 3 and 5 times for R = -1 and R = 0.1, respectively.

The differences between predictions and actual fatigue results are on the order of the accuracy of the underlying residual stress and fatigue data, and may be attributed to cumulative error in both the residual stress measurements and fatigue test data. Additional analyses of Ti-6Al-4V and other alloy systems are currently under way to further validate this predictive design procedure.

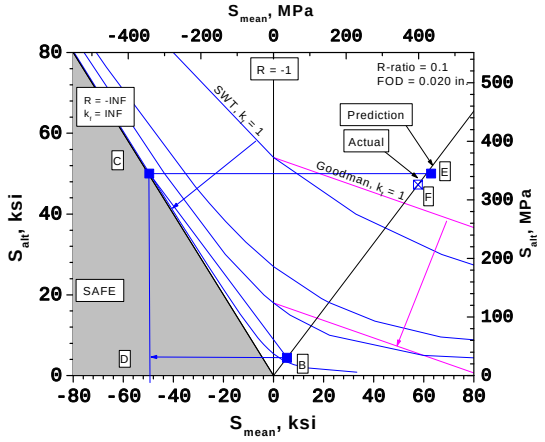

(a)

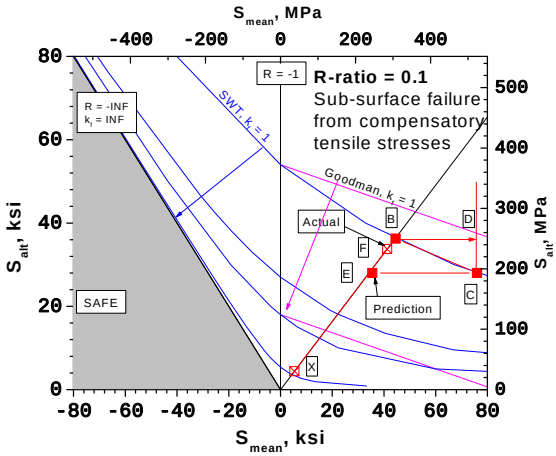

(b)

FIG. 11 - Validation of the design methodology for LPB treated specimens fatigue tested at an R-ratio of 0.1. The design analysis is performed (a) using in FOD initiated failure process, and in (b) using subsurface failure initiation process.

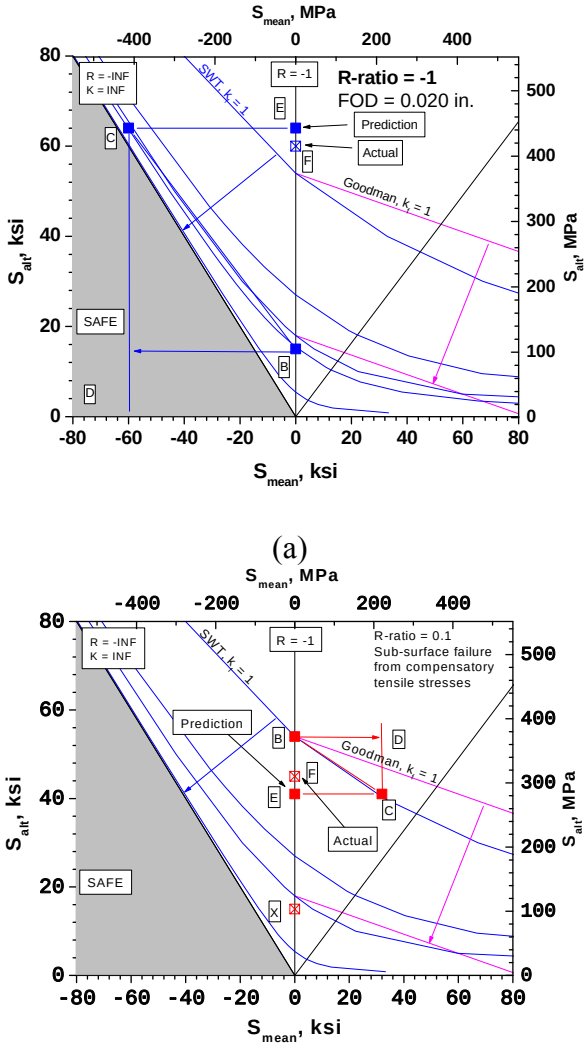

FIG. 12. Validation of the design methodology for LPB treated specimens fatigue tested at an R-ratio for –1. The design analysis is performed (a) using in FOD initiated failure process, and in (b) using subsurface failure initiation process.

SUMMARY AND CONCLUSIONS

A fatigue design method based upon a modified SWT model for unifying fatigue data under various conditions of stress ratio, R, and fatigue notch sensitivity factor, k_f, has been developed.[21] A Fatigue Design Diagram (modified Haigh Diagram) has been developed defining the allowed alternating stress for given applied and residual mean stresses in both the net tensile and compressive mean stress regions. A series of modified SWT lines for various notch sensitivities, k_f, allows the prediction of safe zones. The fatigue design methodology allows the determination of the amount of residual compression that must be introduced into the surface at the depth of fatigue crack initiation to achieve optimum fatigue strength for a given damage state specified by the notch sensitivity, k_f. The method further allows the prediction of surface or subsurface fatigue initiation based upon the measured residual stress field. The proposed fatigue design methodology provides a means to incorporate surface compressive residual stresses imparted through various surface treatments like laser shock peening, low plasticity burnishing, etc., into component design for maximum fatigue benefit. The model has been validated through experimental results for Ti-6Al-4V for R=-1 and 0.1.

ACKNOWLEDGEMENT

The authors wish to gratefully acknowledge constructive discussions and review provided by Dr. Gary Halford of NASA, Glenn Research Center, and Dr. Theodore Nicholas of the Air Force Institute of Technology which have contributed to the development of this paper.

REFERENCE

1. Frost, N.E. Marsh, K.J. Pook, 1974, L.P., *Metal Fatigue*, Oxford University Press
2. Fuchs, H.O. and Stephens, R.I., 1980, *Metal Fatigue In Engineering*, John Wiley & Sons.
3. Berns, H. and Weber, L., 1984, "Influence of Residual Stresses on Crack Growth," Impact Surface Treatment, edited by S.A. Meguid, Elsevier, 33-44.
4. Ferreira, J.A.M., Boorrego, L.F.P., and Costa, J.D.M.,1996, "Effects of Surface Treatments on the Fatigue of Notched Bend Specimens," *Fatigue, Fract. Engng. Mater., Struct.*, Vol. 19 No.1, pp 111-117.
5. Prevéy, P.S. Telesman, J. Gabb, T. and Kantzos, P., March 2000, "FOD Resistance and Fatigue Crack Arrest in Low Plasticity Burnished IN718," Proceedings of the 5th National High Cycle Fatigue Conference, Chandler, AZ.
6. Clauer, A.H., 1996, "Laser Shock Peening for Fatigue Resistance," *Surface Performance of Titanium*, J.K. Gregory, et al, Editors, TMS Warrendale, PA, pp 217-230.
7. P. Prevéy, N. Jayaraman, R. Ravindranath, April 2003, "Effect of Surface Treatments on HCF Performance and FOD Tolerance of a Ti-6Al-4V Vane," Proceedings 8th National Turbine Engine HCF Conference, Monterey, CA.

8. Paul S. Prevéy, et. al., March 2001, "The Effect of Low Plasticity Burnishing (LPB) on the HCF Performance and FOD Resistance of Ti-6Al-4V," Proceedings: 6th National Turbine Engine High Cycle Fatigue (HCF) Conference, Jacksonville, FL.
9. M. Shepard, P. Prevéy, N. Jayaraman, "Effect of Surface Treatments on Fretting Fatigue Performance of Ti-6Al-4V," submitted to International Journal of Fatigue
10. N. Jayaraman, Paul S. Prevéy, Murray Mahoney, March 2003, "Fatigue Life Improvement of an Aluminum Alloy FSW with Low Plasticity Burnishing," Proceedings 132nd TMS Annual Meeting, San Diego, CA.
11. Paul S. Prevéy and John T. Cammett, "The Influence of Surface Enhancement by Low Plasticity Burnishing on the Corrosion Fatigue Performance of AA7075-T6," to appear in International Journal of Fatigue
12. S. Suresh, 2001, *Fatigue of Materials*, Cambridge University Press, p. 226-227
13. H.C. O'Connor, and J.L.M. Morrison, 1956, International Conference on Fatigue, Institution of Mechanical Engineers, pp 102-109.
14. A.R. Woodward, K.W. Gunn and G. Forrest, 1956, "The Effect of Mean Stress on the Fatigue of Aluminum Alloys," International Conference on Fatigue, Institution of Mechanical Engineers, pp 158-170.
15. W.N. Findley, 1954, "Experiments in Fatigue Under Ranges of Stress in Torsion and Axial Load from Tension to Extreme Compression," ASTM, vol. 54, pp 836-846.
16. F.M. Howell and J.L. Miller, 1955, "Axial-Stress Fatigue Strengths of Several Structural Aluminum Alloys," ASEM, vol. 55, pp955-968.
17. K.N. Smith, P. Watson, and T.H. Topper, Dec. 1970, "A Stress-Strain function for the Fatigue of Metals," Journal of Materials, Vol. 5, No. 4, pp 767-778.
18. H.O. Fuchs and R.L. Stephens, 1980, "Metal Fatigue," John Wiley & Sons, New York, p.153.
19. Aerospace Structural Metals Handbook, 3704
20. T. Nicholas and D.C. Maxwell, 2002, "Mean Stress Effects on the High Cycle Fatigue Limit Stress in Ti-6Al-4V," *Fatigue and Fracture Mechanics: 33rd Vol., ASTM STP 1417*, W.G. Reuter and R.S. Piascik, Eds., American Society for Testing and Materials, West Conshohocken, PA.
21. Patent pending.